The fabrication of carbon nanostructures using electron beam resist pyrolysis and nanomachining processes for biosensing applications

2008 Nanotechnology 19 215302

(http://iopscience.iop.org/0957-4484/19/21/215302)

Nanotechnology **19** (2008) 215302 (7pp) doi:10.1088/0957-4484/19/21/215302

The fabrication of carbon nanostructures using electron beam resist pyrolysis and nanomachining processes for biosensing applications

Jung A Lee[1], Kwang-Cheol Lee[2,3], Se Il Park[2] and Seung S Lee[1]

[1] Department of Mechanical Engineering, Korea Advanced Institute of Science and Technology (KAIST), 373-1 Guseong-dong Yuseong-gu, Daejeon 305-701, Republic of Korea
[2] Division of Advanced Technology, Korea Research Institute of Standards and Science (KRISS), 1 Doryong-dong Yuseong-gu, Daejeon 305-340, Republic of Korea

E-mail: kclee@kriss.re.kr

Received 11 July 2007, in final form 6 March 2008
Published 21 April 2008
Online at stacks.iop.org/Nano/19/215302

Abstract
We present a facile, yet versatile carbon nanofabrication method using electron beam lithography and resist pyrolysis. Various resist nanopatterns were fabricated using a negative electron beam resist, SAL-601, and they were then subjected to heat treatment in an inert atmosphere to obtain carbon nanopatterns. Suspended carbon nanostructures were fabricated by the wet-etching of an underlying sacrificial oxide layer. Free-standing carbon nanostructures, which contain 130 nm wide, 15 nm thick, and 4 μm long nanobridges, were fabricated by resist pyrolysis and nanomachining processes. Electron beam exposure dose effects on resist thickness and pattern widening were studied. The thickness of the carbon nanostructures was thinned down by etching with oxygen plasma. An electrical biosensor utilizing carbon nanostructures as a conducting channel was studied. Conductance modulations of the carbon device due to streptavidin–biotin binding and pH variations were observed.

(Some figures in this article are in colour only in the electronic version)

1. Introduction

The detection of chemical or biological species using microfabricated or nanofabricated sensors is currently receiving great attention. In the case of mechanical sensors, microcantilever or nanocantilever bending or resonance frequency changes are monitored by embedded piezoresistors, piezoelectric materials, or strain-sensitive field effect transistors (FETs) [1–6]. Electrical sensors for gas or biomolecule detection have been demonstrated using semiconductor or polymer nanowires, nanotubes, and batch-fabricated silicon FETs [7–13].

Various nanofabrication methods have been pursued for nanodevices and nanoelectromechanical systems (NEMS), as well as for biosensors. Nanomaterial-based devices have active areas below a few tens of nanometers (down to the single molecule level), which are difficult to obtain by top-down fabrication techniques. In addition to the potential of integrated nanodevices and molecular devices, nanomaterial-based devices have unique properties such as ballistic transport, single crystallinity, and quantum phenomena. Despite the promising advantages of nanomaterial-based devices, there are ongoing technological challenges in their manufacture, such as large-scale integration and repeatability.

Silicon or top-down nanofabrication methods have excellent characteristics such as well-established material properties and processes. Although silicon nanodevices have advantages such as batch-fabrication and large-scale integration, increasing process complexity and expensive process equipment for high-fidelity pattern transfer are needed as feature sizes continue to decrease. Low-cost batch-fabrication of arbitrarily shaped, free-standing nanostructures can improve existing nanomaterial- and silicon-based devices and therefore broaden future nanotechnology applications.

[3] Author to whom any correspondence should be addressed.

Carbon thin film, which is fabricated by pyrolysis of patterned resist, shows amorphous graphite-like characteristics with tunable conductivity via pyrolysis temperatures [14, 15]. Because the carbon film is fabricated through a lithography process, we can obtain carbon micro- or nanostructures on a silicon substrate without restrictions in shapes and cross sections, where the feature size is limited by top-down lithography techniques. While the electrochemical behaviors of carbon films in applications such as microbatteries and molecular electronics have been demonstrated, utilization of their mechanical and electrical properties, especially overhanging nanostructures for sensor and actuator applications, is rarely reported [16–19].

The minimum resistivity of carbon films obtained from resist pyrolysis approaches a few mΩ cm, which is comparable to the resistivity of highly doped polysilicon. Resistivity tailoring, from semi-insulating to conducting, is achieved simply by varying pyrolysis temperatures and chemical composition. In conventional NEMS devices, nanostructures are fabricated by etch or deposition steps using photoresists or electron beam resists as masks. The characteristics of pattern transfer fidelity through the resist mask, such as etch selectivity, anisotropy, and etch rate, are important features in NEMS and semiconductor processes. Resists are also used in sacrificial layers as an alternative to silicon oxide in order to fabricate free-standing devices using surface micromachining technology. The resist masks or sacrificial layers are removed by strong acids, solvents, or oxygen plasmas. Resist strip and wafer cleaning are sometimes difficult, especially for a thick resist such as SU-8. The resist itself can be utilized as an active mechanical element in nanoscale devices. With this method, mechanical nanoscale components are fabricated without the necessity for additional deposition and etch processes.

In this paper, we present the fabrication of versatile carbon nanostructures derived from electron beam resist for various sensor and actuator applications, as well as their utilization in biosensors. Various resist shapes, including nanowires and nanodots, were patterned using a negative electron beam resist, SAL-601 (Shipley Co.), and a modified scanning electron microscope (JSM-6400, JEOL). Free-standing nanoscale carbon mechanical structures were fabricated by pyrolysis of the electron beam resist pattern and sacrificial oxide etching. The nanofabrication method eliminates additional processes such as reactive ion etching and provides batch-fabricated, low-cost nanodevices. We also demonstrate streptavidin–biotin binding and pH-dependent conductance modulation using pyrolyzed carbon nanowire devices for biosensors.

2. Device fabrication

2.1. Materials

Phosphate buffered saline solution (PBS, pH 7.4, Bioneer Co.), ethanol (C_2H_5OH, 99.9%), 1-ethyl-3-(3-dimethylaminopropyl) carbodiimide hydrochloride (EDC, Aldrich), and N-hydroxysuccinimide (NHS, Aldrich) were used in this experiment. The amine-conjugated biotin (EZ-Link amine-PEO_2-biotin) and streptavidin (MW = 528 00) were purchased from Pierce and Sigma, respectively. Streptavidin concentrated at 1 mg ml^{-1} in PBS (pH 7.4) was prepared and kept frozen. The frozen streptavidin solution was diluted to 0.5 mg ml^{-1} before use in PBS (pH 7.4).

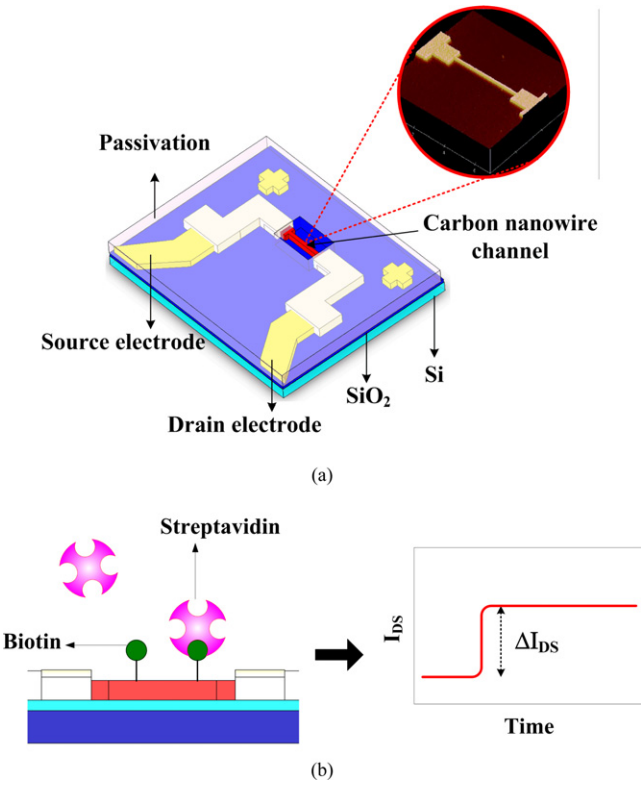

Figure 1. (a) Schematics of an electrical biosensor utilizing carbon nanostructures fabricated from resist pyrolysis as a conducting channel. The carbon nanostructures are connected to source and drain electrodes. The device, except for the carbon nanowire channel, is covered with a passivation layer to shield the metal electrodes against electrolytes. (b) Schematics of variations of source-to-drain current I_{DS} (right) due to streptavidin (target molecule) binding with biotin (receptor molecule) on carbon channels (left).

2.2. Fabrication processes

Figure 1 shows schematic views of the electrical biosensor utilizing carbon nanostructures fabricated from resist pyrolysis as a conducting channel. The carbon nanostructures are connected to source and drain electrodes (figure 1(a)). The device, except for the carbon channels, is covered with a passivation layer to protect the metal electrodes against electrolytes and to reduce nonspecific binding. When target molecules (streptavidin) bind with receptor molecules (biotin) on the carbon nanowire channel, the channel conductance is varied by the charges of the target molecules (streptavidin) (figure 1(b)).

Figure 2 shows the fabrication processes of nanoscale carbon devices for biosensing applications. The fabrication process starts with the growth of 0.8 μm thick SiO_2 by thermal oxidation onto a 4 inch boron-doped (100) Si wafer. The thermal oxide was used as a barrier against carbon diffusion during resist pyrolysis and as an electrical insulation layer. A 70 nm thick Au layer over a 10 nm thick Cr

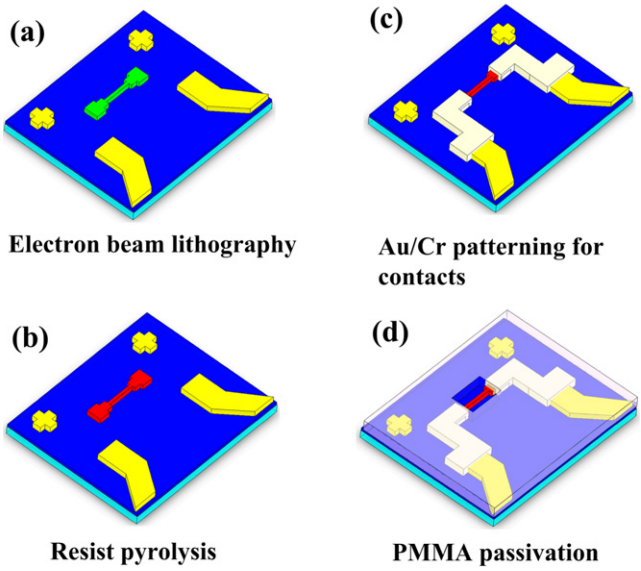

Figure 2. Fabrication processes of carbon nanodevices: (a) resist patterning by electron beam lithography, (b) resist pyrolysis to obtain carbon nanopatterns, (c) metal interconnections between carbon nanopatterns and source/drain electrodes, and (d) passivations of metal electrodes against electrolytes or wet oxide etchant.

layer, for aligning markers for electron beam lithography and source/drain electrodes, was delineated using the lift-off technique. A negative electron beam resist, SAL-601 (Shipley Co.), was spin-coated onto the wafer at 5000 rpm for 35 s, followed by a soft-bake on a hotplate at 170 °C for 3 min. Electron beam resist patterns were fabricated through exposures at 30 keV energy, 0.2–1 μC cm^{-2} doses, and development with AZ300MIF for 5 min (figure 2(a)). We located the resist patterns onto a flat Si region covered only with SiO_2, and not directly onto metal surfaces. When resist patterns are formed on prefabricated metal electrodes, they are liable to be open-circuited after pyrolysis because the resist is thinner near the metal edge due to step coverage problems, and it reflows during heat cycles.

After resist patterning using electron beam lithography, carbon patterns were obtained by resist pyrolysis (figure 2(b)). Several pinholes in the Au/Cr electrodes were observed after resist pyrolysis. Leakage current between electrodes due to carbon or metal diffusion was not observed. We believe that the pinholes in the electrodes are caused by metal agglomeration or melting, and are not caused by metal diffusion through the Cr and SiO_2 barrier. High-temperature-resistant materials such as polysilicon or silicides can be used to eliminate pinholes in prefabricated electrodes. Electron beam exposures for metal contacts were carried out at 30 keV energy with a 100 μC cm^{-2} dose using 950 K 4 wt% polymethyl methacrylate (PMMA). After development in an MIBK solution for 20 s, carbon nanopatterns were connected to source and drain electrodes via the Au/Cr layer through the lift-off technique (figure 2(c)). PMMA passivations followed in order to shield the metal electrodes from liquids (figure 2(d)). Suspended carbon mechanical nanostructures were fabricated by etching the underlying oxide layer using buffered HF.

Figure 3 shows schematics of the experimental setup and temperature profile used in the resist pyrolysis process. Samples with resist nanopatterns were loaded horizontally using a quartz boat into a quartz tube furnace filled with nitrogen gas flows at room temperature. After low-temperature annealing at 300 °C for 3 h, resist pyrolysis was conducted at temperatures between 640 and 760 °C for 30 min. According to the results of thermo-gravimetric analysis (TGA) experiments by ourselves and other groups, weight losses of resists below 500 °C were above 45%, and the first maxima of differential weight loss occur below 200 °C [19]. We carried out low-temperature annealing to reduce organic volatiles such as solvent and resist monomers.

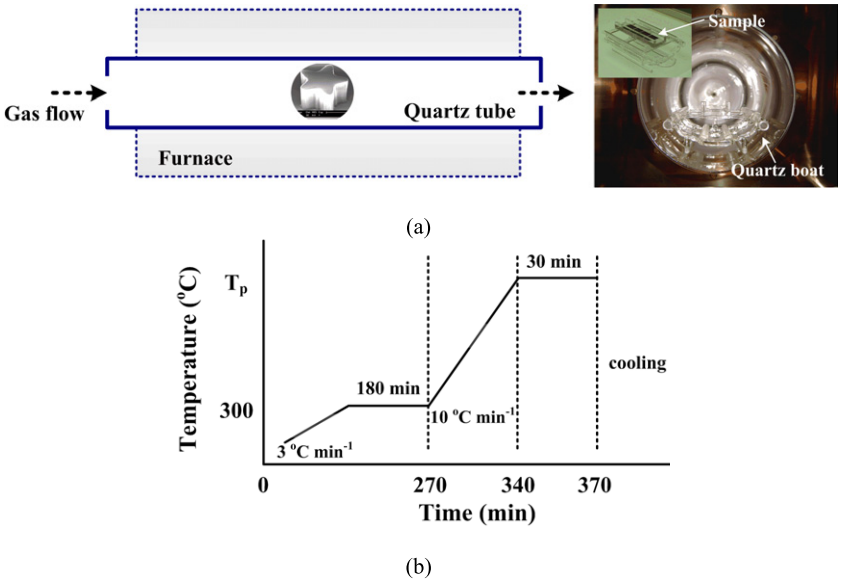

Figure 3. (a) Schematics of the experimental setup and (b) the temperature profile for the resist pyrolysis process. Silicon substrates with patterned resist were loaded into a quartz tube furnace in a nitrogen atmosphere. Resist pyrolysis was carried out for 30 min, following low-temperature annealing for 180 min.

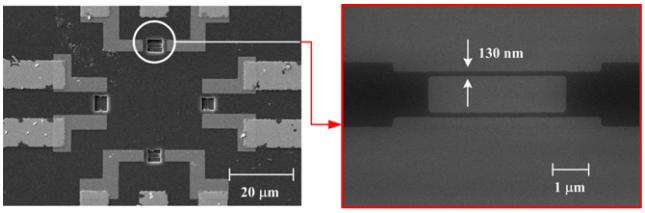

Figure 4. SEM photomicrographs of fabricated carbon devices before the installation of a reservoir.

After PMMA passivation, the device was O_2 plasma-treated at 150 mTorr and 50 W for 15 s to increase the density of oxygen-containing functional groups on the surface of the carbon nanowires. A reservoir was formed using a silicone tube with an inner diameter of 3 mm. By curing a 10:1 mixture of PDMS (Sylgard 184, Dow Corning) at 60 °C for 8 h as a glue, the silicone tube was sealed to the device chip. Figure 4 shows scanning electron microscope (SEM) photomicrographs of the fabricated carbon devices before installation of a reservoir. 130 nm wide, 20 nm thick, and 4 μm long carbon nanowires were connected to the source and drain electrodes. The carbon pattern width was varied to increase the contact area (4 μm × 4 μm) between the carbon and Au/Cr electrodes. Electrical characteristics such as source–drain current, gate-voltage responses, and pH dependences were measured using a semiconductor parameter analyzer (HP4156A).

2.3. Biotin immobilization

Streptavidin, which has a high binding affinity to biotin, was employed as a model protein to demonstrate the utility of carbon nanowires in the proposed biosensor. Biotin, as a receptor for the streptavidin binding measurement, was immobilized on the carbon nanowires. The carbon nanowires were incubated in 100 ml ethanol with 50 mM EDC and 50 mM NHS for 2 h, and were then rinsed with ethanol. The carbon nanowires were kept in 100 ml ethanol with 1 mg ml^{-1} amine-conjugated biotin for 2 h and were then rinsed thoroughly with ethanol and PBS solution (pH 7.4), respectively. The carboxyl (COOH) groups on the surface of the carbon nanowires were transformed using EDC/NHS into intermediates that readily react with the NH_2 groups on biotin. The biotin was immobilized onto the surface of the carbon nanowires using an amide bond.

3. Results

3.1. Carbon nanofabrication

Figure 5(a) shows the thickness and surface roughness of a negative electron beam resist (SAL-601) patterned using different exposure doses. As the exposure dose increases, proximity effects and the molecular weight of the resist also increase due to higher monomer cross-linking. As the dose increased from 0.2 to 1 μC cm^{-2}, the patterned resist thickness increased from 98 to 108 nm, and the surface roughness

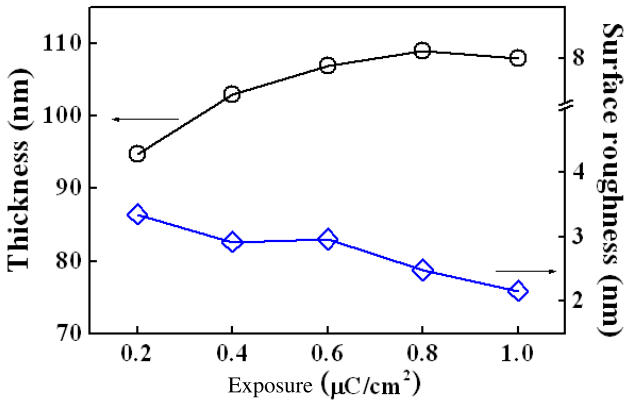

(a)

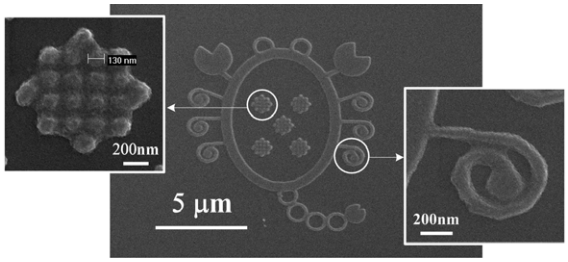

(b)

Figure 5. (a) Negative electron beam resist (SAL-601) pattern thickness and surface roughness variations according to exposure doses between 0.2 and 1 μC cm^{-2}. As the dose increased, the pattern thickness increased, whereas the roughness decreased due to higher monomer cross-linking. (b) An example of fabricated resist patterns using a high dose of 1 μC cm^{-2}. Pattern widening and resist residues were observed due to a higher proximity effect.

decreased from 3.4 to 2.2 nm. Figure 5(b) shows an example of free-style resist nanopatterns fabricated using a 1 μC cm^{-2} dose, which contains 160 nm wide patterns and 65 nm radius dots. Pattern widening and resist residues due to proximity effects were observed in the case of nanopatterns fabricated using a 1 μC cm^{-2} dose (figure 5(b)).

Figure 6 shows examples of free-style resist nanopatterns fabricated from the negative electron beam resist, SAL-601, which shows the versatility of carbon nanofabrication using nanolithography and resist pyrolysis. Curved resist nanopatterns (figures 6(c) and (d)) were fabricated using a low dose of 0.2 μC cm^{-2} to reduce pattern widening and resist residues (scum). The resist nanopatterns were subjected to heat treatment to obtain the intended carbon nanopatterns. Various carbon nanostructures, such as nanowires, nanodots, and suspended nanobridges, were fabricated using this method (figure 7). Because the carbon geometry is defined by the lithography process, we can fabricate carbon devices without restrictions in shape (figures 7(a)–(c)) and 3D mechanical carbon nanostructures (figure 7(d)).

After PMMA passivation to protect the metal electrodes from oxide etchant (figure 2(d)), the underlying oxide was wet-etched using buffered oxide etchant for 3 min. The released carbon nanostructures were rinsed with deionized

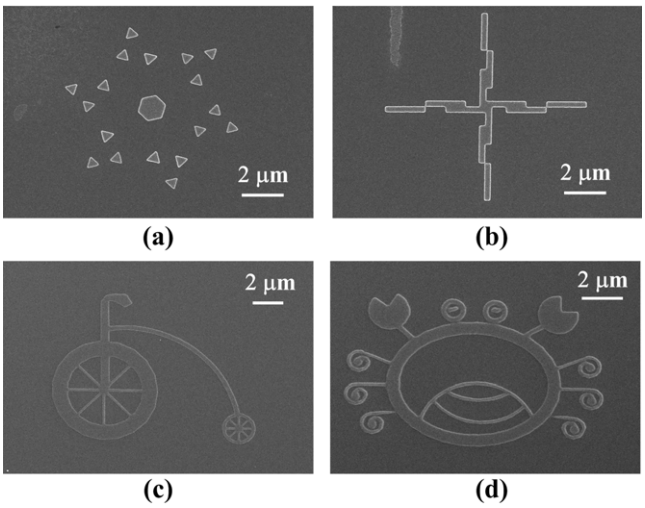

Figure 6. Representative examples of free-style resist nanopatterns, which show the versatility of carbon nanofabrication by resist pyrolysis: (a) triangles, (b) a cross, (c) a bicycle, and (d) a crab which contains 160 nm wide patterns. The resist patterns were fabricated by electron beam lithography with a negative resist, SAL-601. The resist nanopatterns were subjected to heat treatment to obtain designed carbon nanopatterns.

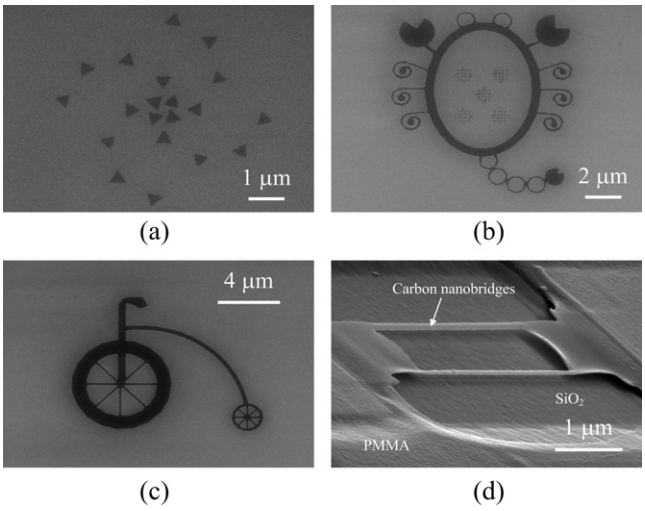

Figure 7. SEM photomicrographs of fabricated carbon nanostructures using electron beam lithography and resist pyrolysis. (a)–(c) are free-handed carbon nanostructures and (d) shows carbon nanobridges suspended over silicon substrate. The carbon nanobridges were fabricated by wet-etching of the underlying oxide layer using buffered HF.

water and methanol and allowed to dry. Figure 7(d) shows 130 nm wide, 15 nm thick, and 4 μm long carbon nanobridges suspended from a silicon substrate fabricated using carbon nanofabrication and underlying oxide etching. The fabricated carbon nanostructures show tensile stresses, useful for mechanical elements such as membranes and bridges, which are formed due to resist shrinkage and outgassing during pyrolysis. The carbon nanobridges can be used as resonant sensors for miniscule force or mass detection. Suspended nanobridges, which have a larger surface-to-volume ratio (a factor of two) compared to nanowires with similar dimensions, will be useful for surface-sensitive devices such as gas sensors and biosensors.

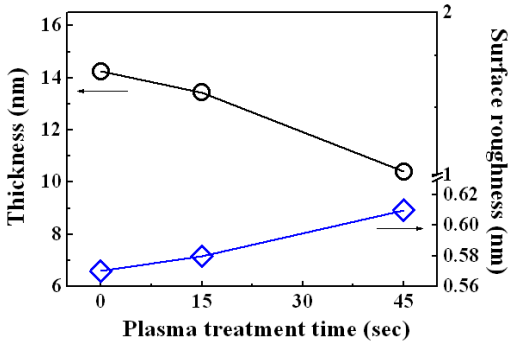

Figure 8. Thickness and roughness variations of carbon nanostructures according to O_2 plasma etching time.

Table 1. Carbon thickness and resistivity variation according to pyrolysis temperatures. The carbon patterns were fabricated through electron beam lithography with a negative resist, SAL-601, and resist pyrolysis at temperatures between 640 and 760 °C.

Pyrolysis temperature (°C)	Carbon thickness (nm)[a]	Thickness ratio (%)[a,b]	Resistivity (Ω cm)[c]
640	21	25	5.2
670	15	16	4.8
700	15	18	4.1
730	18	16	2.3
760	21	24	0.75

[a] Measured by atomic force microscopy.
[b] Carbon thickness after pyrolysis relative to initial resist thickness.
[c] Measured by the van der Pauw method with Greek cross test patterns.

The thickness and surface roughness changes of carbon nanostructures compared to initial resist nanopatterns were measured with an atomic force microscope (AFM, Dimension^{TM} 3100, Digital Instruments). The carbon nanowire thickness fabricated by resist pyrolysis was 25 nm, whereas the initial resist thickness was 100 nm. Carbon thicknesses after pyrolysis were varied by process conditions such as initial resist thickness, exposure doses, and oxidizing gas ratios. Thicker carbon nanostructures were thinned down by oxygen plasma treatment. Resist residues or scum were also removed by oxygen plasma. Figure 8 shows changes in carbon thickness and surface roughness according to the oxygen plasma treatment time. After etching of the carbon nanostructures with oxygen plasma at 50 W for 45 s, the thickness of carbon nanostructures was decreased to 10.4 nm from an initial thickness of 14.3 nm, whereas the surface roughness was slightly increased to 0.61 nm from an initial roughness of 0.57 nm.

Table 1 summarizes the thickness and resistivity variations according to pyrolysis temperatures between 640 and 760 °C for carbon layers fabricated using the negative electron beam resist SAL-601. The carbon thickness and resistivity were measured with the AFM and the van der Pauw method using

Table 2. Hall measurements for carbon layers fabricated by the pyrolysis of negative electron beam resist (SAL-601) patterns at 700 °C (measured with an Accent HL 5500 Hall system).

Pyrolysis temperature (°C)	Carbon thickness (nm)[a]	Carrier concentration (%)	Hall coefficient ($cm^3\ C^{-1}$)	Mobility ($cm^2\ V^{-1}\ s^{-1}$)	Hall voltage (V)
700	20	1.43×10^{19}	0.44	0.11	1.12×10^{-6}

[a] Measured by atomic force microscopy.

Greek cross test patterns, respectively. The thickness of the carbon layer obtained after pyrolysis was between 15 and 21 nm, which was 16–25% of the initial resist thickness of 80–110 nm. The resistivity of the carbon layer was between 5.2 and 0.75 Ω cm, and it decreased as the pyrolysis temperature increased. Black, opaque, smooth carbon surfaces, with a root mean square (rms) roughness below 0.6 nm and indistinguishable top and bottom sides, were obtained using mirror-polished silicon substrates and slow out-gassing during heat treatment. For carbon patterns pyrolyzed at 700 °C, as shown in table 2, a weak p-type majority conduction carrier with a Hall coefficient of 0.44 $cm^3\ C^{-1}$ was measured.

3.2. Streptavidin detection

Many promising applications for nanoscale devices, such as thermistors, heaters, and interconnects, are anticipated using the mechanical and electrical properties of carbon nanostructures. We studied applications of carbon nanostructures to active channels in electrical biosensors. For biosensing applications, we used carbon nanostructures pyrolyzed at 700 °C because of their intermediate conductivity of a few Ω cm and to avoid excess carrier density. Streptavidin (Sigma), which has a high binding affinity to biotin, was employed as a model protein.

Carbon nanostructures containing 20 nm thick, 130 nm wide, and 4 μm thick carbon nanowires were used as conducting channels in the electrical biosensors. Figure 9(a) shows measurements of source-to-drain current I_{DS} versus time for $V_{DS} = 300$ mV after the introduction of 0.5 mg ml^{-1} streptavidin in 10 mM PBS solution (pH 7.4). The source-to-drain current I_{DS} of the biotin-modified carbon nanowire device was increased after streptavidin injection. The increase in I_{DS} after streptavidin introduction can be explained by the effect of negative gate voltages, which are induced by the negative charges of streptavidin (pI = 5) bound with biotin on the carbon nanowires. The increase in I_{DS} after streptavidin introduction was consistent with the results of the Hall measurements showing p-type majority conduction behaviors of the carbon nanostructures.

As a control experiment, streptavidin was introduced to biotin-unmodified carbon nanowire devices. Figure 9(b) shows measurements of I_{DS} versus time with a biotin-unmodified control device for $V_{DS} = 300$ mV after the introduction of 0.5 mg ml^{-1} streptavidin in 10 mM PBS solution (pH 7.4). The I_{DS} values for biotin-unmodified control devices were not changed after streptavidin injection. For negative gate voltages ($V_{GS} < 0$), the drain current I_{DS} for carbon devices after streptavidin injection increased slightly as the gate voltage V_{GS}

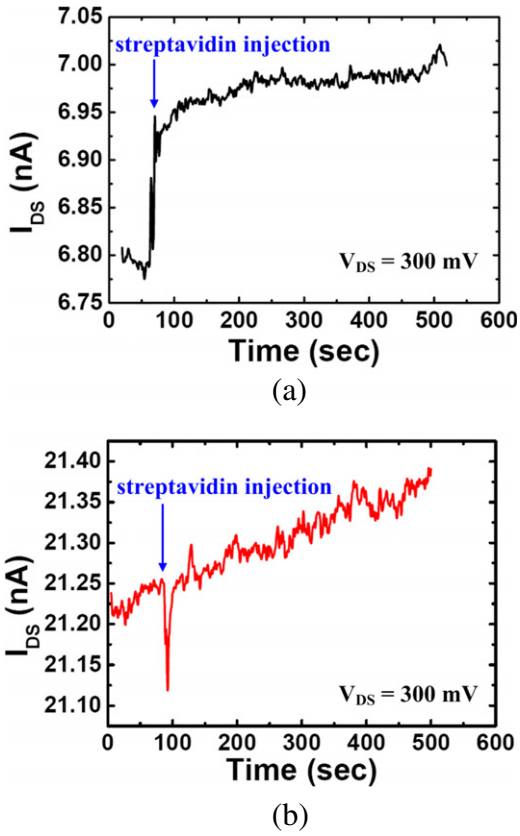

Figure 9. Source-to-drain current (I_{DS}) versus time after streptavidin injection (a) onto a biotin-grafted device and (b) onto biotin-untreated device as a control experiment ($V_{DS} = 300$ mV, ↓: streptavidin injection).

decreased. We believe that the gate-voltage responses can be further improved by modifying the microstructures of the carbon channel. The carbon nanowire device covered with streptavidin/biotin also showed drain conductance variations according to the pH values of buffer solutions. The drain currents I_{DS} of the carbon nanowire devices were decreased as the pH was decreased. At low pH, the positive charges of streptavidin act as positive gate voltages, which reduce carriers in the carbon nanowire devices. Source-to-drain current I_{DS} variations according to streptavidin injections, gate voltages, and pH were demonstrated, which shows binding of streptavidin with biotin on the carbon nanowire devices.

4. Conclusions

We fabricated free-style, free-standing carbon nanostructures, including nanodots, nanowires, and suspended nanobridges, using resist pyrolysis and nanomachining processes. Resist

patterns were fabricated using a negative electron beam resist, SAL-601, and a modified scanning electron microscope (JSM-6400, JEOL). Carbon nanostructures were fabricated by thermal treatment of the resist patterns in a nitrogen atmosphere at temperatures between 640 and 760 °C. Suspended carbon nanobridges were fabricated by wet-etching of the underlying oxide. Electrical biosensors were fabricated by utilizing the carbon nanostructures as conducting channels. The conductances of the carbon nanowire channels were increased after streptavidin injection onto the biotin-grafted devices.

We expect that the carbon nanofabrication method (which relies on resist pyrolysis and a nanomachining process) and the resulting free-standing carbon nanostructures will be useful for various nanoscale sensors, including resonant sensors (mass, force, etc) and biosensors.

Acknowledgment

This work was supported by KOSEF and the Brain Korea 21 program.

References

[1] Wu G, Ji H, Hansen K, Thundat T, Datar R, Cote R, Hagan M F, Chakraborty A K and Majumdar A 2001 Origin of nanomechanical cantilever motion generated from biomolecular interactions *Proc. Natl Acad. Sci. USA* **98** 1560–4

[2] Fritz J, Baller M K, Lang H P, Rothuizen H, Vettiger P, Meyer E, Güntherodt H-J, Gerber Ch and Gimzewski J K 2000 Translating biomolecular recognition into nanomechanics *Science* **288** 316–8

[3] Lavrik N V, Sepaniak M J and Datskos P G 2004 Cantilever transducers as a platform for chemical and biological sensors *Rev. Sci. Instrum.* **75** 2229–53

[4] Abadal G *et al* 2001 Electromechanical model of a resonating nano-cantilever-based sensor for high-resolution and high-sensitivity mass detection *Nanotechnology* **12** 100–4

[5] Shekhawat G, Tark S-H and Dravid V P 2006 MOSFET-embedded microcantilevers for measuring deflection in biomolecular sensors *Science* **311** 1592–5

[6] Truitt P A, Hertzberg J B, Huang C C, Ekinci K L and Schwab K C 2007 Efficient and sensitive capacitive readout of nanomechanical resonator arrays *Nano Lett.* **7** 120–6

[7] Hahm J and Lieber C M 2004 Direct ultrasensitive electrical detection of DNA and DNA sequence variations using nanowire nanosensors *Nano Lett.* **4** 51–4

[8] Ramanathan K, Bangar M A, Yun M, Chen W, Myung N V and Mulchandani A 2005 Bioaffinity sensing using biologically functionalized conducting-polymer nanowire *J. Am. Chem. Soc.* **127** 496–7

[9] Liu H, Kameoka J, Czaplewski D A and Craighead H G 2004 Polymeric nanowire chemical sensor *Nano Lett.* **4** 671–5

[10] Kong J, Franklin N R, Zhou C, Chapline M G, Peng S, Cho K and Dai H 2000 Nanotube molecular wires as chemical sensors *Science* **287** 622–5

[11] So H-M, Won K, Kim Y H, Kim B-K, Ryu B H, Na P S, Kim H and Lee J-O 2005 Single-walled carbon nanotube biosensors using aptamers as molecular recognition elements *J. Am. Chem. Soc.* **127** 11906–7

[12] Li Z, Chen Y, Li X, Kamins T I, Nauka K and Williams R S 2004 Sequence-specific label-free DNA sensors based on silicon nanowires *Nano Lett.* **4** 245–7

[13] Koo S M, Li Q, Edelstein M D, Richter C A and Vogel E M 2005 Enhanced channel modulation in dual-gated silicon nanowire transistors *Nano Lett.* **5** 2519–23

[14] Kostecki R, Schnyder B, Alliata D, Song X, Kinoshita K and Kötz R 2001 Surface studies of carbon films from pyrolyzed photoresist *Thin Solid Films* **396** 36–43

[15] Kim J, Song X, Kinoshita K, Madou M and White R 1998 Electrochemical studies of carbon films from pyrolyzed photoresist *J. Electrochem. Soc.* **145** 2314–9

[16] Schueller O J A, Brittain S T and Whitesides G M 1999 Fabrication of glassy carbon microstructures by soft lithography *Sensors Actuators* A **72** 125–39

[17] Ranganathan S, Steidel I, Anariba F and McCreery R L 2001 Covalently bonded organic monolayers on a carbon substrate: a new paradigm for molecular electronics *Nano Lett.* **1** 491–4

[18] Wang C, Jia G, Taherabadi L H and Madou M J 2005 A novel method for the fabrication of high-aspect ratio C-MEMS structures *J. Microelectromech. Syst.* **14** 348–58

[19] Lee J A, Lee S W, Lee K-C, Park S I and Lee S S 2008 Fabrication and characterization of freestanding 3D carbon microstructures using multi-exposure and resist pyrolysis *J. Micromech. Microeng.* **18** 035012